OPEN

NPG Asia Materials (2017) 9, e340; doi:10.1038/am.2016.195
www.nature.com/am

ORIGINAL ARTICLE

A bipolar nitronyl nitroxide small molecule for an all-organic symmetric redox-flow battery

Tino Hagemann[1,2], Jan Winsberg[1,2], Bernhard Häupler[1,2], Tobias Janoschka[1,2], Jeremy J Gruber[1,2,3], Andreas Wild[1,2] and Ulrich S Schubert[1,2]

An all-organic symmetric redox-flow battery (RFB) that employs nitronyl nitroxide (NN) units as a bipolar redox-active charge-storage material was designed and investigated. An organic molecule possessing two bipolar redox-active NN units connected via a tetraethylene glycol chain was synthesized for this purpose. Owing to the ethylene glycol chain, this molecule demonstrates good solubility in organic solvents. The electrochemical behavior of the obtained compound was investigated via cyclic voltammetry (CV) measurements and it features quasi-reversible redox reactions of the NN^{+}/NN redox couple at $E_{1/2} = 0.37$ V and the NN/NN^{-} redox couple at $E_{1/2} = -1.25$ V versus $AgNO_3$/Ag, which led to a promising cell voltage of 1.62 V in a subsequent battery application. A static solution-based battery exhibits a stable charge/discharge performance over 75 consecutive cycles with a high energy efficiency of 82% and an overall energy density of the electrolyte system of 0.67 W h l^{-1}. In addition, a pumped RFB test demonstrates an overall energy density of the electrolyte system of 4.1 W h l^{-1} and an energy efficiency of 79%.

NPG Asia Materials (2017) **9,** e340; doi:10.1038/am.2016.195; published online 13 January 2017

INTRODUCTION

State-of-the-art redox-flow batteries (RFBs) such as the well-investigated all-vanadium RFB[1–4] contain metal salts and corrosive acidic electrolytes. As these metals are generally obtained as products of mining, their relative abundance in the lithosphere does not represent their actual availability and the process to achieve pure materials such as cobalt and vanadium is expensive. As part of the global energy transition, new energy-storage technologies such as RFBs will increase in popularity. Therefore, the demand for charge-storage materials will grow significantly and, consequently, the price of these metals will rise.[5,6] Further disadvantages of classical RFBs are the deficient civil and environmental standards associated with ore mining, the applied hazardous and highly corrosive acidic electrolytes, and the expensive membranes such as the commonly used Nafion (DuPont, Wilmington, DE, USA) cation-exchange membrane.[6–10]

The development of an all-organic RFB with inexpensive and sustainable redox-active materials and low-cost membranes may overcome these drawbacks.[7,10–14] Among others, Darling *et al.*[15] conducted cost analyses, which revealed that the price of the active material itself and the membrane represent the main costs of these systems. Cost-efficient organic charge-storage materials can feature a price advantage compared with metal-based RFBs; in particular, if the raw materials are affordable, no synthesis or fewer synthesis procedures are required and the avoidance of elaborate purification steps can be achieved. For example, a brief calculation for the anthraquinone disulphonate/bromine system yields a price of $27 per kW h for the redox-active organic charge-storage materials used, which is significantly lower than the price of $81 per kW h for vanadium systems.[16]

In recent years, several semi-organic,[17–29] metal-free organic/inorganic[16,30] and all-organic RFBs[7,11–13,31–35] have been reported. Commonly, two different redox-active materials are used as charge-storage materials, one within the catholyte and the other within the anolyte. To the best of our knowledge, along with Oh *et al.*,[35] Potash *et al.*[14] and Duan *et al.*,[36] we are the only researchers that have used one organic bipolar material simultaneously as both the catholyte and anolyte. Oh *et al.*[35] fabricated a polythiophene microparticle suspension-based electrolyte using polythiophene as the bipolar charge-storage material and at a current density of 0.5 mA cm^{-2} they demonstrated a non-aqueous all-organic RFB with 20 stable charge/discharge cycles, an energy efficiency of 60.9% and an energy density of 2.7 W h l^{-1}. Potash *et al.*,[14] on the other hand, described the bipolar redox-active molecule Disperse Blue 134, a diaminoanthraquinone derivative, and reported a symmetric all-organic solution-based battery in an H-cell glass setup, which exhibits three charge/discharge cycles with an energy efficiency between 43 and 28%, and an energy density

[1]Laboratory of Organic and Macromolecular Chemistry, Institute of Organic Chemistry and Macromolecular Chemistry (IOMC), Jena Center for Soft Matter (JCSM), Friedrich Schiller University Jena, Jena, Germany and [2]Center for Energy and Environmental Chemistry Jena (CEEC Jena), Friedrich Schiller University Jena, Jena, Germany
[3]Current address: Department of Chemical Engineering, 158 Fenske Laboratory, The Pennsylvania State University, University Park, PA 16802, USA.
Correspondence: Professor Dr US Schubert, Laboratory of Organic and Macromolecular Chemistry, Institute of Organic Chemistry and Macromolecular Chemistry (IOMC), Jena Center for Soft Matter (JCSM), Center for Energy and Environmental Chemistry Jena (CEEC Jena), Friedrich Schiller University Jena, Humboldtstrasse 10, D-07743 Jena, Germany.
E-mail: ulrich.schubert@uni-jena.de
Received 16 August 2016; revised 29 September 2016; accepted 13 October 2016

of 0.94 W h l^{-1}. Similar to our work, Duan *et al.*[36] used a nitronyl nitroxide (NN) radical as the charge-storage material. The reported flow battery that used 0.5 M of the commercially available 2-phenyl-4,4,5,5-tetramethylimidazoline-1-oxyl-oxide with 1 M $TBAPF_6$/acetonitrile as the supporting electrolyte demonstrated over 15 consecutive charge/discharge cycles at a current density of 20 mA cm^{-2}, a coulombic efficiency of ~90%, a voltage efficiency of 67%, an energy efficiency of 60%, an energy density of 9 W h l^{-1} during the charging procedure and an energy density of 5 W h l^{-1} during the discharging procedure, which are far better results than those of the two previously reported symmetric RFBs.[36]

The application of a bipolar redox-active charge-storage material in an RFB has significant advantages, such as the considerably reduced synthesis effort, the simplified flow cell design (as both cell compartments use the same material) and a solution to the problematic cross-contamination, which prevents long-term capacity decay.[1,14,35,37,38] The redox-active unit for our approach is the well-known NN radical, which was first described by Osiecki *et al.*[39] The electrochemical behavior of NN radicals and diradicals has been investigated in detail.[40–44] NNs have been used as organic magnetic materials[45] and ligands for single-chain magnets[46] or single-molecule magnets;[47] furthermore, they have been used as organic memory elements[41] and the charge-storage material in an RFB application due to their *n*- and *p*-type properties.[36] In addition, NN-containing polymers are used as bipolar active electrode materials in all-organic radical batteries.[40,48] Owing to their high chemical reversibility, high cell voltage and electrochemical reversibility, NN-containing molecules represent potential charge-storage materials that can be used as the active material in RFBs. To achieve a high theoretical specific capacity (C_{spec}) and to enhance the solubility in solvents preferred for RFB applications, we designed and synthesized a small molecule with two redox-active NN units connected via a tetraethylene glycol chain.

Consequently, the redox-active molecule **4** was electrochemically characterized and its performance as an active material in a static solution-based and a pumped RFB setup was investigated.

MATERIALS AND METHODS

Materials and chemicals

All starting materials were purchased from commercial sources and were used as obtained. The graphite felt (2.25 × 2.25 × 0.4 cm^3, Sigracell GFA6 EA, SGL Carbon, Wiesbaden, Germany) used and the anion-exchange membrane fumasep FAP-PK-3130 (FuMA-Tech, Bietigheim-Bissingen, Germany) were cut into appropriate pieces.

Methods

The reactions were monitored by thin layer chromatography on 0.2 mm silica gel plates (60 F254, Merck Chemicals GmbH, Darmstadt, Germany) and by gas chromatography–mass spectrometry using a Shimadzu (Kyoto, Japan) GCMS-1-system with a GC-QP2010S-detector and an Agilent DB-5 ms-column. Column chromatography was performed on silica gel 60 (Macherey-Nagel, Düren, Germany). ^1H and ^{13}C nuclear magnetic resonance (NMR) spectra were recorded on a Bruker (Billerica, MA, USA) AC 300 (300 and 75 MHz) spectrometer at 298 K. Chemical shifts are reported in parts per million (p.p.m., δ scale) relative to the residual signal of the deuterated solvent. Elemental analyses were carried out using a Vario ELIII-Elementar Euro (Elementar, Langenselbold, Germany) and an EA-HekaTech (HEKAtech GmbH, Wegberg, Germany). Electrospray ionization (ESI) mass spectrometry measurements were performed on a micrOTOF (Bruker) ESI time-of-flight (ESI-TOF) system.

Electrochemical characterization

The radical content of **4** was determined via X-band electron paramagnetic resonance (EPR) spectroscopy. The measurements were conducted on an EMXmicro CW-EPR spectrometer from Bruker using powdered samples and 10^{-4} M solutions in toluene. Samples were investigated at room temperature and data handling was performed on the Bruker Xenon software package, version 1.1b86. The Spin Count software module (Bruker) was used for quantitative measurements. The spectrometer was calibrated using TEMPO (99% (high-performance liquid chromatography) purity, Sigma-Aldrich (St Louis, MO, USA)) as a reference standard. The total spin count provided in this contribution is the average of four measurements. Cyclic voltammetry (CV) and rotating disc electrode (RDE) measurements were conducted on a Model SP-50 potentiostat/galvanostat (Bio-Logic, Seyssinet-Pariset, France), with a glassy carbon tip (5 mm diameter), an $AgNO_3$/Ag reference electrode for organic-based electrolytes and a platinum wire counter electrode. The rotation speed was controlled externally by a Model CTV 101 ring-disk electrode system (Radiometer Analytical SAS, Lyon, France). Evaluation of the RDE analysis via Levich plots (limiting current i_{lim} versus square root of rotation speed ω) yields the diffusion coefficient D by using the Levich equation, $i_{lim} = 0.62\,nFAD^{\frac{2}{3}}\omega^{\frac{1}{2}}\upsilon^{-\frac{1}{6}}c_0$,with $n=1$, Faraday's constant $F=96\,485$ C mol^{-1}, electrode surface area $A=0.2$ cm^2, the kinematic viscosity of the solution $\nu=4.48\times10^{-7}$ m^2 s^{-1} at 298.3 K[49] and the bulk concentration c_0 of the redox-active NN units. As the peak current i_p grows linearly with the square root of the scan rate, the diffusion coefficient D was calculated using the Randles–Sevcik equation, $i_p = 0.4463\,nFAc(nF\nu D)^{\frac{1}{2}}(RT)^{-\frac{1}{2}}$, with $n=1$, Faraday's constant $F=96\,485$ C mol^{-1}, electrode surface area $A=0.2$ cm^2, the bulk concentration c of the redox-active NN units at a temperature $T=298.3$ K and gas constant $R=8.314$ J K^{-1} mol^{-1}.

Cell assembly

The static laboratory cell was designed and constructed into a flat cell type with a membrane active area of 5 cm^2 (JenaBatteries GmbH, Jena, Germany). Supplementary Figure S4 gives a detailed overview of the cell structure. The graphite felt (2.25 × 2.25 × 0.4 cm^3, Sigracell GFA6 EA, SGL Carbon) and anion-exchange membrane fumasep FAP-PK-3130 (FuMA-Tech) were cut into appropriate pieces. Charge/discharge tests were conducted on a VMP3 potentiostat/galvanostat (Bio-Logic). To study the impact of the current density on the battery performance, dynamic measurements were performed. The electrolyte was circulated between the electrochemical cell and the storage tanks with a peristaltic pump (Hei-FLOW Value 01 Multi, Heidolph, Schwabach, Germany). Typically, 4 or 10 ml of the electrolyte was used with a flow rate of 10 ml min^{-1}. All measurements were carried out at 25 °C under argon atmosphere in a glove box. The batteries were charged/discharged with constant current and the resulting potential was measured over time.

Synthesis of the NN containing compound 4

Compound **1** was prepared with slight modifications according to the procedure from Hirel *et al.*[50]

2,3-Dimethyl-2,3-dinitrobutane (17.85 g, 0.1 mol) was suspended in concentrated hydrochloric acid (37%, 150 ml). The suspension was heated up to 50 °C and granular tin (100 g, 0.84 mol) was added in portions over a period of one hour. Subsequently, the suspension was heated to 90 °C for 4 h and stirred at 110 °C until the mixture became a clear solution. After cooling to room temperature, the solution was extracted with diethyl ether (100 ml, three times), to remove residual 2,3-dimethyl-2,3-dinitrobutane. Afterwards, saturated sodium hydroxide solution (150 ml) was added to the aqueous phase under cooling in an ice bath. The resulting black precipitate was removed by filtration and the clear solution obtained was extracted with CH_2Cl_2 (100 ml, three times). The combined organic phases were dried over $MgSO_4$ and then the solvent was removed under reduced pressure to obtain **1** as a colorless solid (5.24 g, 0.045 mol) in a yield of 45%. ^1H NMR (300 MHz, $CDCl_3$, δ): 1.24 (brs, 4H, NH_2), 1.08 (s, 12H, CH_3); ^{13}C NMR (75 MHz, $CDCl_3$, δ): 54.66 (CC), 26.41 (CH_3); ESI-TOF MS *m/z* (%): 117.14 (100) $[M^+ + H]$; high resolution mass spectrometry (ESI) *m/z*: $[M + H]^+$ calcd for $C_6H_{16}N_2$, 117.1386; found, 117.1383.

Compound **2** was prepared with slight modifications according to the procedure from Wang *et al.*[51]

Under inert conditions, K_2CO_3 (42.1 g, 0.305 mol) and 4-hydroxybenzaldehyde (18.6 g, 0.152 mol) were dissolved in dry dimethylformamide (230 ml) and 1-chloro-2-[2-[2-(2-chloroethoxy)ethoxy]ethoxy]ethane (13.6 ml,

0.069 mol) was added dropwise. The solution was stirred at 120 °C for 20 h. After cooling to room temperature, the solvent was removed under reduced pressure. The oily residue was diluted in $CHCl_3$ (10 ml), whereby the remaining K_2CO_3 precipitated as a white solid. The K_2CO_3 was filtered off and the filtrate was dried over Na_2SO_4. The solvent was removed under reduced pressure to obtain the crude product, which was purified via column chromatography (SiO_2; ethyl acetate: *n*-heptane 5:1) to obtain the pure product **2** (21.35 g, 0.053 mol) in a yield of 77%. ^{1}H NMR (300 MHz, $CDCl_3$, δ): 9.85 (s, 2H; CHO), 7.79 (d, $J=9$ Hz, 4H, Ar H), 6.99 (d, $J=9$ Hz, 4H, Ar H), 4.18 (t, $J=6$ Hz, 4H, CH_2), 3.86 (t, $J=6$ Hz, 4H, CH_2), 3.70–3.68 (m, 8H, CH_2); ^{13}C NMR (75 MHz, $CDCl_3$, δ): 190.85 (C=O), 163.88 (CO), 132.00 (CC), 130.11 (CC), 114.93 (CC), 70.58 (CO), 70.72 (CO), 69.53 (CO), 67.82 (CO); ESI-TOF MS *m/z* (%): 425.36 (100) [M^+ + Na], 403.83 (16) [M^+ + H]; high resolution mass spectrometry (ESI) *m/z*: [M + Na]$^+$ calcd for $C_{22}H_{26}O_7$, 425.1570; found, 425.1561; Anal. calcd. for $C_{22}H_{26}O_7$: C 65.66, H 6.51; found: C 65.76, H 6.54.

Compound **3** was prepared as follows.

Compound **1** (5.2 g, 0.045 mol) was dissolved in tetrahydrofuran (100 ml) and a solution of **2** (8.6 g, 0.021 mol) in tetrahydrofuran (50 ml) was added dropwise. The reaction mixture was stirred at room temperature until the condensation was completed (monitored via thin layer chromatography). The solvent was removed *in vacuo* to obtain a yellowish oil, which solidified overnight at 5 °C. The solid was washed with diethyl ether (30 ml, three times) to obtain **3** as a white powder (10.3 g, 0.017 mol) in a yield of 81%. ^{1}H NMR (300 MHz, $CDCl_3$, δ): 7.43 (d, $J=9$ Hz, 4H, Ar H), 6.85 (d, $J=9$ Hz, 4H, Ar H), 5.12 (s, 2H, CH), 4.09 (t, $J=6$ Hz, 4H, CH_2), 3.83 (t, $J=6$ Hz, 4H, CH_2), 3.69 to 3.68 (m, 8H, CH_2), 2.09 (s, 4H, CH_2), 1.17 (s, 12H, CH_3), 1.09 (s, 12H, CH_3); ^{13}C NMR (75 MHz. $CDCl_3$, δ): 158.33 (CO), 136.37 (CC), 127.61 (CC), 114.52 (CC), 73.05 (CC), 70.93 (CO), 70.78 (CO), 69.85 (CO), 67.56 (CO), 62.92 (CC), 25.6 (CH_3), 23.77 (CH_3); ESI-TOF MS *m/z* (%): 599.40 (8) [M^+ + H], 300.21 (100) [M^{2+} + H]; high resolution mass spectrometry (ESI) *m/z*: [M + H]$^{2+}$ calcd for $C_{34}H_{54}N_4O_5$, 300.2119; found, 300.2113; Anal. calcd. for $C_{34}H_{54}N_4O_5$: C 68.20; H 9.09; N 9.36; found: C 68.20; H 9.07; N 8.91.

Compound **4** was prepared as follows.

A mixture of 4,4'-[oxy*bis*(2,1-ethanediyloxy-2,1-ethanediyloxy)]*bis*-4,4,5,5-tetramethylimidazolidine (**3**, 10 g, 0.017 mol), CH_2Cl_2 (500 ml) and saturated $NaHCO_3$ solution (300 ml) was cooled to 0 °C. Over a period of 1 h, a solution of *m*-chloroperbenzoic acid (⩽77%, 14.64 g, 0.085 mol) in CH_2Cl_2 (180 ml) was added dropwise to the reaction mixture. Subsequently, a solution of $NaIO_4$ (10.89 g, 0.051 mol) in water (180 ml) was added dropwise. The mixture was allowed to reach room temperature and was stirred for an additional hour. Then, the organic phase was separated from the aqueous phase and the aqueous solution was extracted with CH_2Cl_2 (three times). Subsequently, the combined organic phases were extracted with saturated $NaHCO_3$ (200 ml). The organic phase was dried over Na_2SO_4, filtered and concentrated under reduced pressure. The resulting crude purple residue was purified *via* column chromatography (SiO_2; ethyl acetate) to yield **4** (3.65 g, 0.0056 mol, 33%) as a purple oil. ESI-TOF MS *m/z* (%): 656.34 (100) [$M^{2\bullet+}$]; high resolution mass spectrometry (ESI) *m/z*: [M]$^+$ calcd for $C_{34}H_{48}N_4O_9^{2\bullet}$, 656.3415; found, 656.3402; Anal. calcd. for $C_{34}H_{48}N_4O_9^{2\bullet}$: C 62.18, H 7.37, N 8.53; found: C 62.63; H 7.38; N 7.60; EPR: calcd spin-activity for $C_{34}H_{48}N_4O_9^{2\bullet}$: 97.31%.

RESULTS AND DISCUSSION

Synthesis and electrochemical behavior of 4

For battery applications, the active material used should possess a high energy density. Therefore, the theoretical specific capacity, the cell voltage and, in particular, the solubility of the redox-active material in the applied solvent should be maximized. Unfortunately, most aromatic NNs exhibit a moderate to poor solubility in nitrile- and carbonate-based solvents, which are preferred for RFB applications due to their electrochemical stability. To improve the solubility and thereby the energy density, even compared with the commercial available 2-phenyl-4,4,5,5-tetramethylimidazoline-1-oxyl-oxide, an ethylene glycol chain was introduced as a linker between two NN molecules. It is noteworthy that due to the presence of two NN units per molecule, the theoretical capacity and the solubility compared with the single NN units is doubled. The introduction of two redox-active NN units was performed to achieve a high theoretical specific capacity by improving the solubility of molecule **4** in preferred organic solvents, such as acetonitrile (3.8 molal). Furthermore, the synthesis of the active dimeric material was beneficial in comparison with a monomeric active material. The starting material used, 1-chloro-2-[2-[2-(2-chloroethoxy)ethoxy]ethoxy]ethane, has several benefits such as a reasonable price per kg or the absence of interfering hydroxyl end groups, for example, 1-chloro-2-[2-(2-methoxyethoxy)ethoxy]ethane, 1-chloro-2-[2-(2-ethoxyethoxy)ethoxy]ethane or 2-[2-[2-(2-chloroethoxy)ethoxy]ethoxy]ethanol. Based on its good chemical stability in acetonitrile, benzonitrile and carbonate-based solvents, a fumasep FAP-PK-3130 (FuMA-Tech) anion-exchange membrane was used to separate the electrolyte circuits. In contrast to commonly used Nafion membranes, this simpler membrane presents a high cost-saving potential. Acetonitrile was selected for all static and pumped flow battery tests, as it demonstrated the highest solubility of **4** and the best PF_6^- ion transport across the membrane, which resulted in a low electric cell resistance (determined by electrochemical impedance spectroscopy (Supplementary Figure S6a and b).

A higher theoretical specific capacity may be achieved by using 2,2'-[oxy*bis*(2,1-ethanediyloxy)]*bis*acetaldehyde as the linker unit to obtain an NN-containing molecule with a theoretical specific capacity of 120.7 mA h g^{-1}. Unfortunately, this compact NN-containing molecule is not practical for battery applications due to its poor chemical stability in solution in the presence of air. Various studies show that the introduction of an aromatic ring (C_6H_4R) at the 2-position of the NN moiety leads to a significantly enhanced stability of the radicals against the presence of air.[52–54] Therefore, it is essential to introduce a phenyl spacer between the NN units and the solubility-promoting tetraethylene glycol linker to engineer stable NN-containing small molecules. With 1-chloro-2-[2-[2-(2-chloroethoxy)ethoxy]ethoxy] ethane as the starting compound, this is, in the simplest case, the 4,4'-[oxy*bis*(2,1-ethanediyloxy-2,1-ethanediyloxy)]*bis*nitronylnitroxide (**4**) with a theoretical specific capacity of 81.7 mA h g^{-1} (Scheme 1).

Compound **4** was obtained from inexpensive commercially available starting materials in four synthesis steps (Scheme 1). Here, 2, 3-dimethyl-2,3-dinitrobutane was completely reduced (Sn/conc. HCl, reflux) to achieve the corresponding diamino compound **1** in a moderate yield of 45%.[50] The *bis*aldehyde **2** was prepared from 4-hydroxybenzaldehyde and 1-chloro-2-[2-[2-(2-chloroethoxy) ethoxy]ethoxy]ethane under inert conditions in dry dimethylformamide. K_2CO_3 was used as a base to obtain **2** in a yield of 77%.[51] The subsequent condensation reaction of **1** and **2** in tetrahydrofuran produced compound **3** in a yield of 81%. In the last reaction step, the *bis*imidazolidine **3** was oxidized in a one-pot reaction, first by *meta*-chloroperbenzoic acid to the *bis*hydroxyimidazolidine and, subsequently, by sodium periodate to the NN redox-active material **4** in a moderate yield of 33%.[50] A brief calculation of the costs of this bipolar redox-active charge-storage material can be found in the Supplementary Information.

The unpaired electrons of the two NN groups of molecule **4** were characterized by EPR spectroscopy. The EPR spectrum, obtained in 10^{-4} M toluene solution, displays a nine-line pattern in the hyperfine structure (Figure 1a). According to the literature, a five-line pattern with an intensity ratio of 1:2:3:2:1 is expected due to the interaction between the two identical nitrogens of the NN group. However, because of the close proximity of the two NN units in compound **4**, a spin–spin interaction between both NN units occurs, which results in

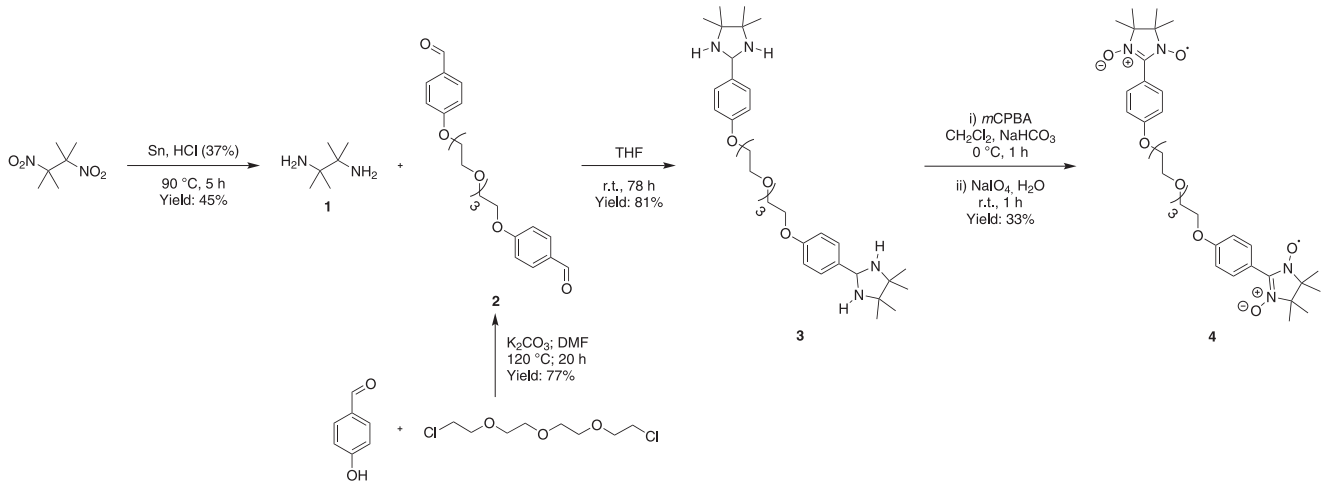

Scheme 1 Schematic representation of the synthesis route for the nitronyl nitroxide-containing compound **4**.

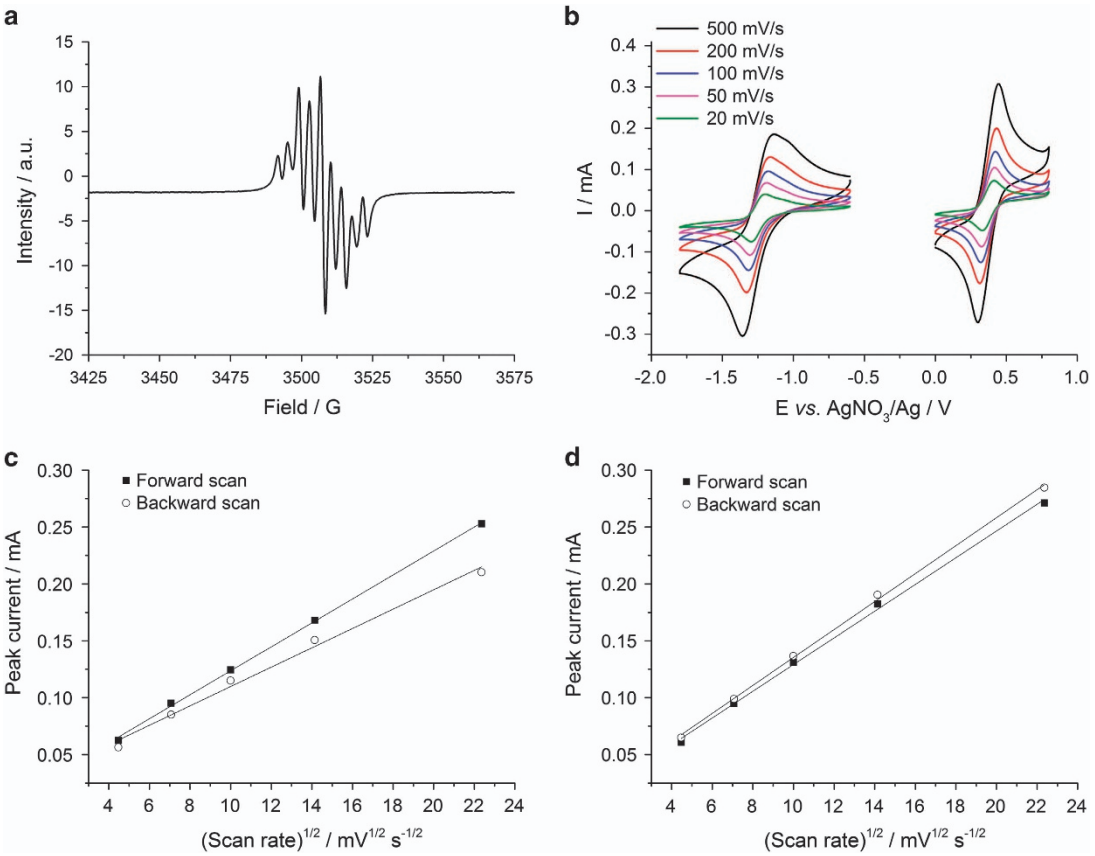

Figure 1 Characterization of **4**: (**a**) EPR spectrum of **4** in 10^{-4} M toluene solution, (**b**) cyclic voltammogram obtained for 2.1 mM CH_3CN solution of **4** with 0.1 M $TBAPF_6$ as the supporting electrolyte at different scan rates, (**c**) plot of the reduction and the re-oxidation peak current versus square root of the scan rate and (**d**) plot of the oxidation and the re-reduction peak current versus square root of the scan rate.

a nine-line pattern.[40,55] The absolute spin activity of compound **4**, obtained from the EPR spectrum in solid state (Supplementary Figure S1), was 1.79×10^{18} spins per mg, which equals a radical content of above 97% and indicates a complete oxidation of *bis*imidazolidine.

The electrochemical properties of NN radicals and diradicals are well known, and they have been investigated in detail in previous reports.[40–44] Several studies show that the electrochemical behavior of the NNs strongly depends on the substituent. For example, Sukegawa *et al.*[40] reported a phenyl-substituted NN diradical that can undergo reversible oxidation and reduction reactions.

The electrochemical properties of compound **4** were investigated via CV, to determine the formal potentials of the NN redox couples, and RDE measurements, to obtain the diffusion coefficient and the rate constant. The CV measurements of compound **4** were performed in acetonitrile solution with 0.1 M $TBAPF_6$ as a conductive salt. The cyclic

voltammogram (Figure 1b) displays a quasi-reversible oxidation and re-reduction of the NN to the oxoammonium cation (NN^+) at $E_{½} = 0.37$ V versus $AgNO_3$/Ag with a peak split of 146 mV and a quasi-reversible reduction and re-oxidation of the NN to the aminoxyl anion (NN^-) at $E_{½} = -1.25$ V versus $AgNO_3$/Ag with a peak split of 218 mV, which would lead to a cell voltage of 1.62 V in a subsequent battery application. At approximately −1 V at the re-oxidation of the reduction of the NN to the NN^-, a second minor peak is visible, which indicates possible side reactions and/or consecutive reactions of the NN^-. A more extensive investigation of the CV curves (Figure 1c and d) for both redox couples, the NN^+/NN and the NN/NN^-, exhibits a linear relation between the peak currents and the square root of the scan rate, which reveals a diffusion-controlled behavior and the non-appearance of precipitates. Using the Randles–Sevcik equation, the diffusion coefficients D of 1.08×10^{-5} and 0.81×10^{-5} cm^2 s^{-1} were calculated for the NN^+/NN and NN/NN^- redox couples, respectively. The obtained diffusion coefficient D for both these redox couples is in the same magnitude as the diffusion coefficient D subsequently calculated by using the Levich equation from the evaluation of the RDE measurements.

RDE measurements of **4** were performed in acetonitrile solution with 0.1 M $TBAPF_6$ as the supporting electrolyte for the oxidation to the oxoammonium cation (NN^+, Supplementary Figure S2 and Supplementary Information) and the reduction to the NN^- (Supplementary Figure S3 and Supplementary Information). The NN^+/NN redox couple exhibits a diffusion-controlled behavior of **4** with a diffusion coefficient D of 4.74×10^{-6} cm^2 s^{-1} (Supplementary Figure S2a and b, and Supplementary Information). Subsequently, the Koutecký–Levich analysis performed displays mass-transport-independent currents and the following Tafel analysis (Supplementary Figure S2c and d, and Supplementary Information) presents an electron-transfer rate constant (k^0) of 1.42×10^{-2} cm s^{-1} and a transfer coefficient α of 0.59, which is close to the α-value of an ideal reversible redox-reaction of 0.5.

The NN/NN^- redox couple also exhibits a diffusion-controlled behavior of **4** in acetonitrile with 0.1 M $TBAPF_6$ and a diffusion coefficient D of 3.45×10^{-6} cm^2 s^{-1} (Supplementary Figure S3a and b, and Supplementary Information). Unfortunately, both the Koutecký–Levich analysis and the Tafel analysis could not be performed. We assume that the calculation of the kinetics of the redox-reaction was impossible due to the non-defined redox-reaction of the NN/NN^- redox couple. The cyclic voltammogram (Figure 1b) of the reduction of the NN to the NN^- and the corresponding re-oxidation, in contrast to the NN^+/NN redox couple, displays a broader peak split, a large peak width and, at lower scan rates, a slight potential shift, which leads to a non-defined redox reaction. This issue can be caused by side reactions and/or consecutive reactions of the NN^-. To summarize, the diffusion coefficient D obtained for the NN/NN^+ and the NN/NN^- redox couple, and the electron-transfer rate constant k^0 and the transfer coefficient α for the NN/NN^+ redox couple are similar to the values reported in the literature for other organic charge-storage materials, such as the comparable 2-phenyl-4,4,5,5-tetramethylimidazoline-1-oxyl-oxide material,[36] DBBB[32,56] and several quinone derivatives;[16,33,57] thereby, they enable the application of **4** in a battery test cell.

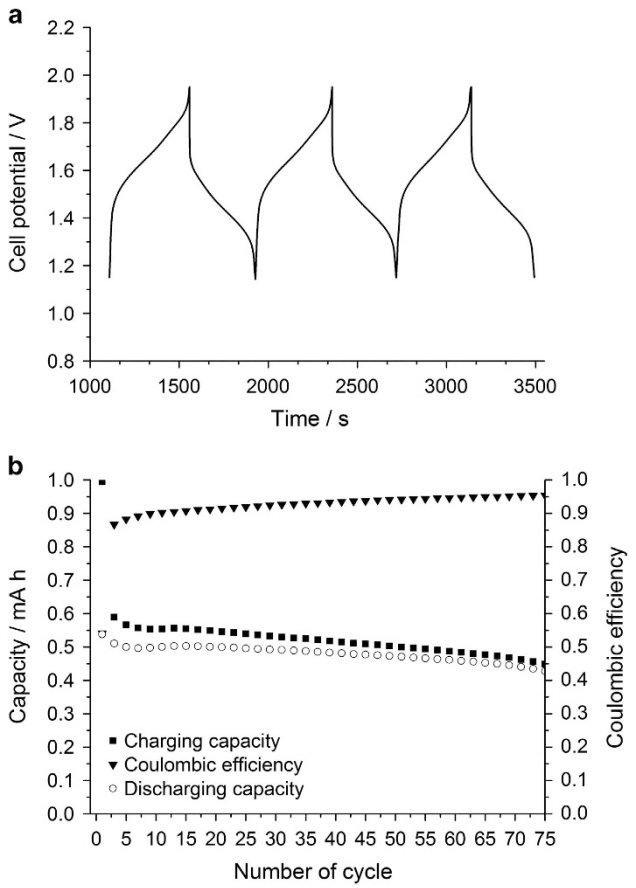

Figure 2 Charge/discharge experiments in a 5 cm^2 electrochemical static test cell with 16 mM (32 mM NN units) **4** and 0.5 M $TBAPF_6$ in acetonitrile, (**a**) representative third to fifth charge/discharge cycles at a current density of 1 mA cm^{-2} and (**b**) long-time stability: charge and discharge capacity and columbic efficiency at a current density of 1 mA cm^{-2}.

Battery tests

The use of compound **4** as a bipolar charge-storage material for RFB applications was initially investigated in a static battery setup (Supplementary Figure S4 and Supplementary Information). Here, acetonitrile with 0.5 M $TBAPF_6$ was used as the supporting electrolyte and a fumasep anion-exchange membrane was applied to separate the cathode and anode compartments.

The static solution-based battery comprised a 16 mM (32 mM active NN units) solution of **4** within the anolyte and catholyte. This results in a theoretical capacity of 0.88 A h l^{-1} for both solutions and an overall energy density of the electrolyte system of 0.67 W h l^{-1}. The charge/discharge experiments were conducted in a voltage range of 1.10–1.95 V and a stable battery cycling was performed for 75 consecutive charge/discharge cycles at a current density of 1 mA cm^{-2}. Representatively, cycles 3 to 5 are shown in Figure 2a.

The NN-containing static solution-based battery exhibits well-defined charge and discharge plateaus at 1.67 and 1.45 V, respectively. Coulombic efficiencies up to 95% were attained, which indicate a good chemical reversibility of the redox reactions of the bipolar charge-storage material and a low membrane crossover. A voltage efficiency of 86% and an energy efficiency of 82% were exemplarily calculated for the 75th cycle. For the static battery setup used, a theoretical discharge capacity of 1.97 mA h is possible, whereas a discharge capacity of 0.53 mA h (27%) could be achieved in the first cycle (Figure 2b) at a current density of 1 mA cm^{-2}. This moderate material activity originates from the use of un-pumped battery setup, where only a limited amount of the redox-active NN units can be transported to the active electrode area by diffusion. In addition to this kinetic limitation, a high overpotential further reduces the material

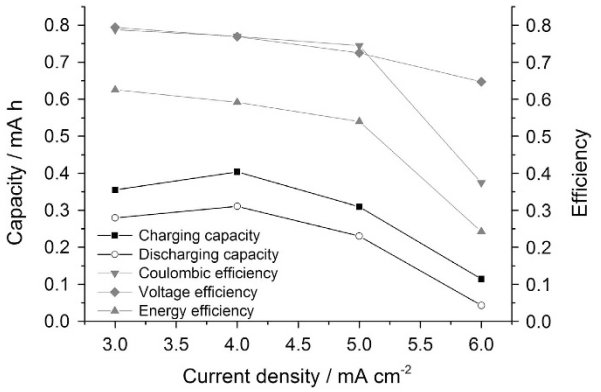

Figure 3 Electric performance of a pumped 5 cm^2 test cell with 16 mM (32 mM NN units) **4** and 0.5 M $TBAPF_6$ in acetonitrile (with a theoretical capacity of 0.83 A h l^{-1} for both solutions); capacity, coulombic, voltage and energy efficiency with respect to the current density for 10 ml electrolyte per half-cell, with the flow rate adjusted to 10 ml min^{-1}.

activity and the cell design allows only a rough estimation of the electrolyte volume. Furthermore, after 75 consecutive charge/discharge cycles, a capacity decay of ~20% was observed (Figure 2a), which is probably caused by side reactions of the charged species or decomposition by the reaction of radicals with each other.

To determine the impact of the current density on the performance of the flow battery, charge/discharge measurements in a pumped flow battery (Supplementary Figure S5 and Supplementary Information) were performed (Figure 3).

Four different current densities (3, 4, 5 and 6 mA cm^{-2}) were applied, and the charge/discharge capacity and the coulombic, voltage and energy efficiency were determined. The capacity decreases linearly as the current density increases, except for the current density of 3 mA cm^{-2}, due to the limited mass transport to the electrode, which leads to an increasing overpotential. Charging/discharging was possible up to current densities of 6 mA cm^{-2}. At this current density, the coulombic efficiency drops significantly under 40% because of kinetic limitations in the discharging process. In addition, with increasing current densities, a linear decline of the voltage efficiency was observed, which is presumably induced by the restricted ion conductivity in the applied electrolyte and, therefore, by the increasing potential gap between the charging and discharging plateaus.

In addition, further pumped flow battery tests with a higher concentration of the active material **4** were performed (Figure 4). This battery comprised 0.1 M (0.2 M active NN units) **4** and 0.5 M $TBAPF_6$ in acetonitrile, as the anolyte and catholyte, respectively, resulting in a theoretical capacity of 5.4 A h l^{-1} for both solutions and an overall energy density of the electrolyte system of 4.1 W h l^{-1}. The charge/discharge experiments were conducted in a voltage range from 1.10 to 1.95 V and battery cycling was performed for 20 consecutive charge/discharge cycles at a current density of 1 mA cm^{-2}.

At an active material concentration of 0.1 M (0.2 M active NN units), the electrolyte viscosity increased during the charging process, which resulted in an impaired mass transport and a high overvoltage and eventually caused a low material utilization (~20%) and a steep voltage profile (Figure 4a). The change in viscosity is attributed to a decrease in the solubility of the charged species in contrast to the pristine active material **4**. Furthermore, after 11 consecutive charge/discharge cycles, a capacity fade of approximately 50%, probably due to side reactions of the charged species or decomposition by the reaction of radicals with each other, was observed (Figure 4b). It is noteworthy that up to

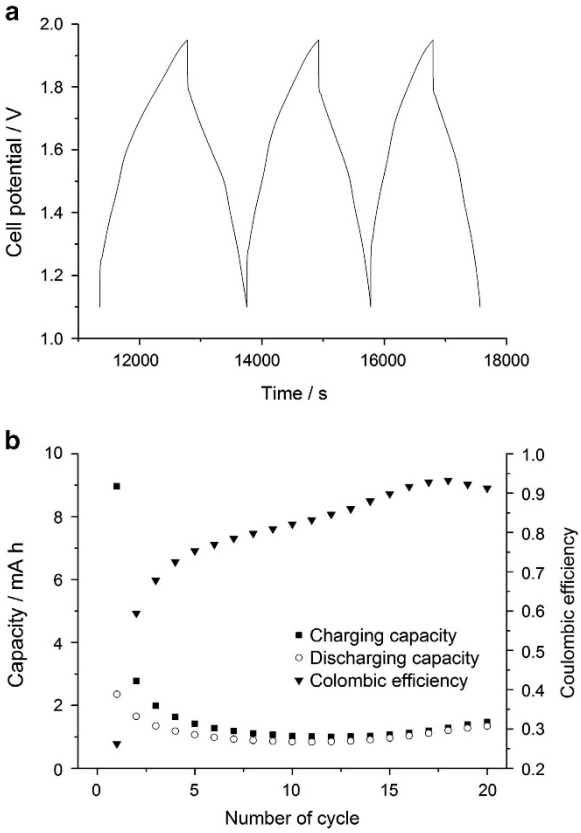

Figure 4 Charge/discharge experiments in a pumped 5 cm^2 electrochemical test cell with 0.1 M (0.2 M NN units) **4** and 0.5 M $TBAPF_6$ in acetonitrile, (**a**) representative third to fifth charge/discharge cycles at a current density of 1 mA cm^{-2}, and (**b**) charge and discharge capacity and columbic efficiency at a current density of 1 mA cm^{-2} over 20 charge/discharge cycles.

cycle 20, the capacity recovers to ~60% of the original value because the pumped cell requires some time to reach the ideal operational conditions. This can be attributed to the decrease of the area-specific resistance, from 2.58 Ω before cycling to 1.91 Ω after cycling (Supplementary Figure S6 and Supplementary Information), which results in a subsequently achieved cutoff voltage that leads to a higher material utilization. At 0.5 M (1 M active NN units) **4**, the charged species precipitated and therefore the charged active material (Supplementary Figure S7) cannot be discharged at higher concentrations.

The maximum solubility limit (3.8 M in acetonitrile) of **4** in pumped flow battery experiments was not attained. This was probably because the two charged NN units reduced the solubility of **4** in the electrolyte used. The use of a longer ethylene glycol chain, a detailed optimization of the electrolyte and an improvement in the cell design may solve this limitation.

CONCLUSION

An all-organic RFB with a bipolar molecule containing two redox-active NN units was successfully demonstrated. Compound **4** was synthesized in four synthesis steps from inexpensive commercially available materials. Two NNs were connected via a tetraethylene glycol chain, which improves the solubility behavior to 3.8 molal in the preferred organic solvent, acetonitrile. Compound **4** was electrochemically characterized via CV, which shows a quasi-reversible redox reaction at $E_{½} = 0.37$ V for the NN^+/NN and at $E_{½} = -1.25$ V versus $AgNO_3/Ag$ for the NN/NN^- redox couple, leading to a high cell

voltage of 1.62 V and RDE measurements, which display a diffusion-controlled behavior. Furthermore, its potential as a bipolar charge-storage material for RFB applications was demonstrated in a static and pumped laboratory test cell. The static flow battery was charged/discharged at a current density of 1 mA cm^{-2} for 75 consecutive cycles and it achieved coulombic efficiencies of up to 95%, a voltage efficiency of 86% and an energy efficiency of 82%. The pumped battery test revealed stable capacity retention and efficiencies for current densities in the range of 3 to 5 mA cm^{-2}.

According to these preliminary static and pumped battery tests, which exhibit far better results than those from the previously reported symmetric RFBs by Oh *et al.*[35] and Potash *et al.*,[14] and are comparable to values for symmetric RFB described by Duan *et al.*,[36] compound **4** appears to possess a high potential for the application as a bipolar organic charge-storage material in non-aqueous all-organic RFBs. However, further investigations are required to improve certain properties, for example, the solubility of the charged species, to achieve higher energy densities and performance parameters. This can be conducted by a detailed optimization of the electrolyte.

CONFLICT OF INTEREST

The authors declare no conflict of interest.

ACKNOWLEDGEMENTS

We thank the European Regional Development Fund (EFRE), the Thuringian Ministry for Economic Affairs, Science and Digital Society (TMWWdG), the Zentrales Innovationsprogramm Mittelstand (ZIM) and the Fonds der Chemischen Industrie (FCI) for the financial support, René Burgés for electrospray ionization mass spectrometry measurements, Sabine Morgenstern for EPR measurements, Christian Friebe for help with the electrochemical characterization and JenaBatteries GmbH for the redox-flow cell assembly.

1 Skyllas-Kazacos, M., Rychcik, M., Robins, R. G. & Fane, A. G. New all-vanadium redox flow cell. *J. Electrochem. Soc.* **133**, 1057–1058 (1986).
2 Vijayakumar, M., Wang, W., Nie, Z., Sprenkle, V. & Hu, J. Elucidating the higher stability of vanadium(V) cations in mixed acid based redox flow battery electrolytes. *J. Power Sources* **241**, 173–177 (2013).
3 Roe, S., Menictas, C. & Skyllas-Kazacos, M. A high energy density vanadium redox flow battery with 3 M vanadium electrolyte. *J. Electrochem. Soc.* **163**, A5023–A5028 (2016).
4 Sun, C., Chen, J., Zhang, H., Han, X. & Luo, Q. Investigations on transfer of water and vanadium ions across Nafion membrane in an operating vanadium redox flow battery. *J. Power Sources* **195**, 890–897 (2010).
5 Barnhart, C. J. & Benson, S. M. On the importance of reducing the energetic and material demands of electrical energy storage. *Energy Environ. Sci.* **6**, 1083–1092 (2013).
6 Armand, M. & Tarascon, J. M. Building better batteries. *Nature* **451**, 652–657 (2008).
7 Janoschka, T., Martin, N., Martin, U., Friebe, C., Morgenstern, S., Hiller, H., Hager, M. D. & Schubert, U. S. An aqueous, polymer-based redox-flow battery using non-corrosive, safe, and low-cost materials. *Nature* **527**, 78–81 (2015).
8 Weber, A., Mench, M., Meyers, J., Ross, P., Gostick, J. & Liu, Q. Redox flow batteries: a review. *J. Appl. Electrochem.* **41**, 1137–1164 (2011).
9 Zhang, X., Yang, L., Li, Y., Li, H., Wang, W. & Ye, B. Impacts of lead/zinc mining and smelting on the environment and human health in China. *Environ. Monit. Assess.* **184**, 2261–2273 (2012).
10 Winsberg, J., Hagemann, T., Janoschka, T., Hager, M. D. & Schubert, U. S. Redox-flow batteries: from metals to organics. *Angew. Chem. Int. Ed.* doi:10.1002/anie.201604925R201604921 (2016).
11 Janoschka, T., Morgenstern, S., Hiller, H., Friebe, C., Wolkersdorfer, K., Haeupler, B., Hager, M. D. & Schubert, U. S. Synthesis and characterization of TEMPO- and viologen-polymers for water-based redox-flow batteries. *Polym. Chem.* **6**, 7801–7811 (2015).
12 Liu, T., Wei, X., Nie, Z., Sprenkle, V. & Wang, W. A Total organic aqueous redox flow battery employing a low cost and sustainable methyl viologen anolyte and 4-HO-TEMPO catholyte. *Adv. Energy Mater.* **6**, 1501449 (2016).
13 Wei, X., Xu, W., Huang, J., Zhang, L., Walter, E., Lawrence, C., Vijayakumar, M., Henderson, W. A., Liu, T., Cosimbescu, L., Li, B., Sprenkle, V. & Wang, W. Radical compatibility with nonaqueous electrolytes and its impact on an all-organic redox flow battery. *Angew. Chem. Int. Ed.* **54**, 8684–8687 (2015).
14 Potash, R. A., McKone, J. R., Conte, S. & Abruña, H. D. On the benefits of a symmetric redox flow battery. *J. Electrochem. Soc.* **163**, A338–A344 (2016).
15 Darling, R. M., Gallagher, K. G., Kowalski, J. A., Ha, S. & Brushett, F. R. Pathways to low-cost electrochemical energy storage: a comparison of aqueous and nonaqueous flow batteries. *Energy Environ. Sci.* **7**, 3459–3477 (2014).
16 Huskinson, B., Marshak, M. P., Suh, C., Er, S., Gerhardt, M. R., Galvin, C. J., Chen, X., Aspuru-Guzik, A., Gordon, R. G. & Aziz, M. J. A metal-free organic-inorganic aqueous flow battery. *Nature* **505**, 195–198 (2014).
17 Xu, Y., Wen, Y., Cheng, J., Cao, G. & Yang, Y. Study on a single flow acid Cd-chloranil battery. *Electrochem. Commun.* **11**, 1422–1424 (2009).
18 Xu, Y., Wen, Y.-H., Cheng, J., Cao, G.-P. & Yang, Y.-S. A study of tiron in aqueous solutions for redox flow battery application. *Electrochim. Acta* **55**, 715–720 (2010).
19 Wang, W., Xu, W., Cosimbescu, L., Choi, D., Li, L. & Yang, Z. Anthraquinone with tailored structure for a nonaqueous metal-organic redox flow battery. *Chem. Commun.* **48**, 6669–6671 (2012).
20 Wei, X., Xu, W., Vijayakumar, M., Cosimbescu, L., Liu, T., Sprenkle, V. & Wang, W. TEMPO-based catholyte for high-energy density nonaqueous redox flow batteries. *Adv. Mater.* **26**, 7649–7653 (2014).
21 Huang, J., Cheng, L., Assary, R. S., Wang, P., Xue, Z., Burrell, A. K., Curtiss, L. A. & Zhang, L. Liquid catholyte molecules for nonaqueous redox flow batteries. *Adv. Energy Mater.* **5**, 1401782 (2015).
22 Huang, J., Su, L., Kowalski, J. A., Barton, J. L., Ferrandon, M., Burrell, A. K., Brushett, F. R. & Zhang, L. A subtractive approach to molecular engineering of dimethoxybenzene-based redox materials for non-aqueous flow batteries. *J. Mater. Chem. A* **3**, 14971–14976 (2015).
23 Lin, K., Chen, Q., Gerhardt, M. R., Tong, L., Kim, S. B., Eisenach, L., Valle, A. W., Hardee, D., Gordon, R. G., Aziz, M. J. & Marshak, M. P. Alkaline quinone flow battery. *Science* **349**, 1529–1532 (2015).
24 Takechi, K., Kato, Y. & Hase, Y. A highly concentrated catholyte based on a solvate ionic liquid for rechargeable flow batteries. *Adv. Mater.* **27**, 2501–2506 (2015).
25 Zhao, Y., Si, S. & Liao, C. A single flow zinc//polyaniline suspension rechargeable battery. *J. Power Sources* **241**, 449–453 (2013).
26 Nagarjuna, G., Hui, J., Cheng, K. J., Lichtenstein, T., Shen, M., Moore, J. S. & Rodríguez-López, J. Impact of redox-active polymer molecular weight on the electrochemical properties and transport across porous separators in nonaqueous solvents. *J. Am. Chem. Soc.* **136**, 16309–16316 (2014).
27 Sukegawa, T., Masuko, I., Oyaizu, K. & Nishide, H. Expanding the dimensionality of polymers populated with organic robust radicals toward flow cell application: synthesis of TEMPO-crowded bottlebrush polymers using anionic polymerization and ROMP. *Macromolecules* **47**, 8611–8617 (2014).
28 Winsberg, J., Muench, S., Hagemann, T., Janoschka, T., Morgenstern, S., Billing, M., Schacher, F. H., Hauffman, G., Gohy, J.-F., Hoeppener, S., Hager, M. D. & Schubert, U. S. Polymer/zinc hybrid-flow battery using block copolymer micelles featuring a TEMPO corona as catholyte. *Polym. Chem.* **7**, 1711–1718 (2016).
29 Winsberg, J., Janoschka, T., Morgenstern, S., Muench, S., Hagemann, T., Hauffman, G., Gohy, J.-F., Hager, M. D. & Schubert, U. S. Poly(TEMPO)/zinc hybrid-flow battery: a novel, 'green,' high voltage, and safe energy storage system. *Adv. Mater.* **28**, 2238–2243 (2016).
30 Chen, Q., Gerhardt, M. R., Hartle, L. & Aziz, M. J. A quinone-bromide flow battery with 1 W cm^{-2} power density. *J. Electrochem. Soc.* **163**, A5010–A5013 (2016).
31 Li, Z., Li, S., Liu, S., Huang, K., Fang, D., Wang, F. & Peng, S. Electrochemical properties of an all-organic redox flow battery using 2,2,6,6-tetramethyl-1-piperidinyloxy and N-methylphthalimide. *Electrochem. Solid State Lett.* **14**, A171–A173 (2011).
32 Brushett, F. R., Vaughey, J. T. & Jansen, A. N. An all-organic non-aqueous lithium-ion redox flow battery. *Adv. Energy Mater.* **2**, 1390–1396 (2012).
33 Yang, B., Hoober-Burkhardt, L., Wang, F., Surya Prakash, G. K. & Narayanan, S. R. An inexpensive aqueous flow battery for large-scale electrical energy storage based on water-soluble organic redox couples. *J. Electrochem. Soc.* **161**, A1371–A1380 (2014).
34 Kaur, A. P., Holubowitch, N. E., Ergun, S., Elliott, C. F. & Odom, S. A. A highly soluble organic catholyte for non-aqueous redox flow batteries. *Energy Technol.* **3**, 446–446 (2015).
35 Oh, S. H., Lee, C. W., Chun, D. H., Jeon, J. D., Shim, J., Shin, K. H. & Yang, J. H. A metal-free and all-organic redox flow battery with polythiophene as the electroactive species. *J. Mater. Chem. A* **2**, 19994–19998 (2014).
36 Duan, W., Vemuri, R. S., Milshtein, J. D., Laramie, S., Dmello, R. D., Huang, J., Zhang, L., Hu, D., Vijayakumar, M., Wang, W., Liu, J., Darling, R. M., Thompson, L., Smith, K., Moore, J. S., Brushett, F. R. & Wei, X. A symmetric organic-based nonaqueous redox flow battery and its state of charge diagnostics by FTIR. *J. Mater. Chem. A* **4**, 5448–5456 (2016).
37 Rasmussen, P. G. Electrical Storage Device Vinazene Inc. (Ann Arbor, MI, USA, 2011).
38 Rychcik, M. & Skyllas-Kazacos, M. Characteristics of a new all-vanadium redox flow battery. *J. Power Sources* **22**, 59–67 (1988).
39 Osiecki, J. H. & Ullman, E. F. a-Nitronyl nitroxides, a new class of stable radicals. *J. Am. Chem. Soc.* **90**, 1078–1079 (1968).
40 Sukegawa, T., Kai, A., Oyaizu, K. & Nishide, H. Synthesis of pendant nitronyl nitroxide radical-containing poly(norbornene)s as ambipolar electrode-active materials. *Macromolecules* **46**, 1361–1367 (2013).

41 Lee, J., Lee, E., Kim, S., Bang, G. S., Shultz, D. A., Schmidt, R. D., Forbes, M. D. E. & Lee, H. Nitronyl nitroxide radicals as organic memory elements with both n- and p-type properties. *Angew. Chem. Int. Ed.* **50**, 4414–4418 (2011).
42 Ziessel, R., Ulrich, G., Lawson, C. R. & Echegoyen, L. Oligopyridine bis(nitronyl nitroxides): synthesis, structures, electrochemical, magnetic and electronic properties. *J. Mater. Chem.* **9**, 1435–1448 (1999).
43 Coronado, E., Gimenez-Saiz, C., Nicolas, M., Romero, F. M., Rusanov, E. & Stoeckli-Evans, H. Synthesis, crystal structures and electronic properties of imidazoline nitroxide radicals bearing active groups in electropolymerisation. *New J. Chem.* **27**, 490–497 (2003).
44 Nakano, Y., Yagyu, T., Hirayama, T., Ito, A. & Tanaka, K. Synthesis and intramolecular magnetic interaction of triphenylamine derivatives with nitronyl nitroxide radicals. *Polyhedron* **24**, 2141–2147 (2005).
45 Caneschi, A., Gatteschi, D., Lalioti, N., Sangregorio, C., Sessoli, R., Venturi, G., Vindigni, A., Rettori, A., Pini, M. G. & Novak, M. A. Cobalt(II)-nitronyl nitroxide chains as molecular magnetic nanowires. *Angew. Chem. Int. Ed.* **40**, 1760–1763 (2001).
46 Zhou, S. Y., Li, X., Li, T., Tian, L., Liu, Z. Y. & Wang, X. G. A series of heterospin complexes based on lanthanides and pyridine biradicals: synthesis, structure and magnetic properties. *RSC Adv.* **5**, 17131–17139 (2015).
47 Li, L.-L., Liu, S., Zhang, Y., Shi, W. & Cheng, P. Three new mononuclear tri-spin lanthanide-nitronyl nitroxide radical compounds: syntheses, structures and magnetic properties. *Dalton Trans.* **44**, 6118–6125 (2015).
48 Suga, T., Sugita, S., Ohshiro, H., Oyaizu, K. & Nishide, H. p- and n-Type bipolar redox-active radical polymer: toward totally organic polymer-based rechargeable devices with variable configuration. *Adv. Mater.* **23**, 751–754 (2011).
49 DDBST GmbH http://www.ddbst.com/en/EED/PCP/VSK_C3.php Accessed on 10 August 2016.
50 Hirel, C., Vostrikova, K. E., Pécaut, J., Ovcharenko, V. I. & Rey, P. Nitronyl and Imino nitroxides: improvement of ullman's procedure and report on a new efficient synthetic route. *Chem. Eur. J.* **7**, 2007–2014 (2001).
51 Wang, W. & Li, A. D. Q. Design and synthesis of efficient fluorescent dyes for incorporation into DNA backbone and biomolecule detection. *Bioconjugate Chem.* **18**, 1036–1052 (2007).
52 Ullman, E. F., Call, L. & Osiecki, J. H. Stable Free radicals. VIII. New imino, amidino, and carbamoyl nitroxides. *J. Org. Chem.* **36**, 3623–3631 (1970).
53 Ullman, E. F., Osiecki, J. H., Boocock, D. G. B. & Darcy, R. Studies of stable free radicals. X. Nitronyl nitroxide monoradicals and biradicals as possible small molecule spin labels. *J. Amer. Chem. Soc.* **94**, 7049–7059 (1972).
54 Dulog, L. & Kim, J. S. Stable free radical paramagnetic monomers containing aminoxylamine oxide moieties. An intermediate step toward organic ferromagnetic polyradicals. *Die Makromol. Chem.* **190**, 2609–2614 (1989).
55 Nishide, H., Hozumi, Y., Nii, T. & Tsuchida, E. Poly(1,2-phenylenevinylene)s bearing nitronyl nitroxide and galvinoxyl at the 4-position: π-conjugated and non-kekulé-type polyradicals with a triplet ground state. *Macromolecules* **30**, 3986–3991 (1997).
56 Su, L., Ferrandon, M., Kowalski, J. A., Vaughey, J. T. & Brushett, F. R. Electrolyte development for non-aqueous redox flow batteries using a high-throughput screening platform. *J. Electrochem. Soc.* **161**, A1905–A1914 (2014).
57 Zhang, S., Li, X. & Chu, D. An organic electroactive material for flow batteries. *Electrochim. Acta* **190**, 737–743 (2016).

Supplementary Information accompanies the paper on the NPG Asia Materials website (http://www.nature.com/am)